The Astrophysical Journal Supplement Series, 263:24 (9pp), 2022 December https://doi.org/10.3847/1538-4365/ac9523

The Fourth Catalog of Active Galactic Nuclei Detected by the Fermi Large Area Telescope: Data Release 3

M. Ajello[1], L. Baldini[2], J. Ballet[3], D. Bastieri[4,5,6], J. Becerra Gonzalez[7], R. Bellazzini[8], A. Berretta[9], E. Bissaldi[10,11], R. Bonino[12,13], A. Brill[14,68], P. Bruel[15], S. Buson[16], R. Caputo[14], P. A. Caraveo[17], C. C. Cheung[18], G. Chiaro[17], N. Cibrario[12,13], S. Ciprini[19,20], M. Crnogorcevic[14,21], S. Cutini[22], F. D'Ammando[23], S. De Gaetano[10,11], N. Di Lalla[24], L. Di Venere[10,11], A. Domínguez[25], V. Fallah Ramazani[26], E. C. Ferrara[14,21,27], A. Fiori[2], Y. Fukazawa[28], S. Funk[29], P. Fusco[10,11], V. Gammaldi[30], F. Gargano[11], S. Garrappa[31], D. Gasparrini[19,20], N. Giglietto[10,11], F. Giordano[10,11], M. Giroletti[23], D. Green[32], I. A. Grenier[3], S. Guiriec[14,33], D. Horan[15], X. Hou[34,35], T. Kayanoki[28], M. Kuss[8], S. Larsson[36,37], L. Latronico[12], T. Lewis[14], J. Li[38,39], I. Liodakis[40], F. Longo[41,42], F. Loparco[10,11], B. Lott[43], M. N. Lovellette[44], P. Lubrano[22], G. M. Madejski[24], S. Maldera[12], A. Manfreda[2], G. Martí-Devesa[45], M. N. Mazziotta[11], I. Mereu[9,22], P. F. Michelson[24], N. Mirabal[14,46], W. Mitthumsiri[47], T. Mizuno[48], M. E. Monzani[24,49], A. Morselli[19], I. V. Moskalenko[24], M. Negro[27,46], R. Ojha[14], M. Orienti[23], E. Orlando[24,50], J. F. Ormes[51], Z. Pei[5], H. Peña-Herazo[12,13,52,53,54], M. Persic[42,55], M. Pesce-Rollins[8], V. Petrosian[24], R. Pillera[10,11], H. Poon[28], T. A. Porter[24], G. Principe[23,41,42], S. Rainò[10,11], R. Rando[4,5,6], B. Rani[14,56,57], M. Razzano[2], S. Razzaque[58], A. Reimer[45], O. Reimer[45], L. Scotton[59], D. Serini[11], C. Sgrò[8], E. J. Siskind[60], G. Spandre[8], P. Spinelli[10,11], D. J. Suson[61], H. Tajima[24,62], D. F. Torres[63,64,65], J. Valverde[14,46], H. Yassin[66], and G. Zaharijas[67]

[1] Department of Physics and Astronomy, Clemson University, Kinard Lab of Physics, Clemson, SC 29634-0978, USA
[2] Università di Pisa and Istituto Nazionale di Fisica Nucleare, Sezione di Pisa I-56127 Pisa, Italy
[3] AIM, CEA, CNRS, Université Paris-Saclay, Université de Paris, F-91191 Gif-sur-Yvette, France
[4] Istituto Nazionale di Fisica Nucleare, Sezione di Padova, I-35131 Padova, Italy
[5] Dipartimento di Fisica e Astronomia "G. Galilei", Università di Padova, Via F. Marzolo, 8, I-35131 Padova, Italy
[6] Center for Space Studies and Activities "G. Colombo", University of Padova, Via Venezia 15, I-35131 Padova, Italy
[7] Instituto de Astrofísica de Canarias, Observatorio del Teide, C/Via Lactea, s/n, E-38205 La Laguna, Tenerife, Spain
[8] Istituto Nazionale di Fisica Nucleare, Sezione di Pisa, I-56127 Pisa, Italy
[9] Dipartimento di Fisica, Università degli Studi di Perugia, I-06123 Perugia, Italy
[10] Dipartimento di Fisica "M. Merlin" dell'Università e del Politecnico di Bari, via Amendola 173, I-70126 Bari, Italy
[11] Istituto Nazionale di Fisica Nucleare, Sezione di Bari, I-70126 Bari, Italy
[12] Istituto Nazionale di Fisica Nucleare, Sezione di Torino, I-10125 Torino, Italy
[13] Dipartimento di Fisica, Università degli Studi di Torino, I-10125 Torino, Italy
[14] NASA Goddard Space Flight Center, Greenbelt, MD 20771, USA
[15] Laboratoire Leprince-Ringuet, École polytechnique, CNRS/IN2P3, F-91128 Palaiseau, France
[16] Institut für Theoretische Physik and Astrophysik, Universität Würzburg, D-97074 Würzburg, Germany
[17] INAF-Istituto di Astrofisica Spaziale e Fisica Cosmica Milano, via E. Bassini 15, I-20133 Milano, Italy
[18] Space Science Division, Naval Research Laboratory, Washington, DC 20375-5352, USA
[19] Istituto Nazionale di Fisica Nucleare, Sezione di Roma "Tor Vergata", I-00133 Roma, Italy; stefano.ciprini.asdc@gmail.com, dario.gasparrini@ssdc.asi.it
[20] Space Science Data Center—Agenzia Spaziale Italiana, Via del Politecnico, snc, I-00133, Roma, Italy
[21] Department of Astronomy, University of Maryland, College Park, MD 20742, USA
[22] Istituto Nazionale di Fisica Nucleare, Sezione di Perugia, I-06123 Perugia, Italy
[23] INAF Istituto di Radioastronomia, I-40129 Bologna, Italy
[24] W.W. Hansen Experimental Physics Laboratory, Kavli Institute for Particle Astrophysics and Cosmology, Department of Physics and SLAC National Accelerator Laboratory, Stanford University, Stanford, CA 94305, USA
[25] Grupo de Altas Energías, Universidad Complutense de Madrid, E-28040 Madrid, Spain
[26] Ruhr University Bochum, Faculty of Physics and Astronomy, Astronomical Institute (AIRUB), D-44780 Bochum, Germany
[27] Center for Research and Exploration in Space Science and Technology (CRESST) and NASA Goddard Space Flight Center, Greenbelt, MD 20771, USA
[28] Department of Physical Sciences, Hiroshima University, Higashi-Hiroshima, Hiroshima 739-8526, Japan
[29] Friedrich-Alexander Universität Erlangen-Nürnberg, Erlangen Centre for Astroparticle Physics, Erwin-Rommel-Str. 1, D-91058 Erlangen, Germany
[30] Departamento de Física Teórica, Universidad Autónoma de Madrid, E-28049 Madrid, Spain
[31] Deutsches Elektronen Synchrotron DESY, D-15738 Zeuthen, Germany
[32] Max-Planck-Institut für Physik, D-80805 München, Germany
[33] The George Washington University, Department of Physics, 725 21st Street NW, Washington, DC 20052, USA
[34] Yunnan Observatories, Chinese Academy of Sciences, 396 Yangfangwang, Guandu District, Kunming 650216, People's Republic of China
[35] Key Laboratory for the Structure and Evolution of Celestial Objects, Chinese Academy of Sciences, 396 Yangfangwang, Guandu District, Kunming 650216, People's Republic of China
[36] Department of Physics, KTH Royal Institute of Technology, AlbaNova, SE-106 91 Stockholm, Sweden
[37] The Oskar Klein Centre for Cosmoparticle Physics, AlbaNova, SE-106 91 Stockholm, Sweden
[38] CAS Key Laboratory for Research in Galaxies and Cosmology, Department of Astronomy, University of Science and Technology of China, Hefei 230026, People's Republic of China
[39] School of Astronomy and Space Science, University of Science and Technology of China, Hefei 230026, People's Republic of China
[40] Finnish Centre for Astronomy with ESO (FINCA), University of Turku, FI-21500 Piikiö, Finland
[41] Dipartimento di Fisica, Università di Trieste, I-34127 Trieste, Italy
[42] Istituto Nazionale di Fisica Nucleare, Sezione di Trieste, I-34127 Trieste, Italy
[43] Université Bordeaux, CNRS, LP2I Bordeaux, UMR 5797, F-33170 Gradignan, France; lott@cenbg.in2p3.fr
[44] The Aerospace Corporation, 14745 Lee Road, Chantilly, VA 20151, USA
[45] Institut für Astro- und Teilchenphysik, Leopold-Franzens-Universität Innsbruck, A-6020 Innsbruck, Austria
[46] Department of Physics and Center for Space Sciences and Technology, University of Maryland Baltimore County, Baltimore, MD 21250, USA
[47] Department of Physics, Faculty of Science, Mahidol University, Bangkok 10400, Thailand

[48] Hiroshima Astrophysical Science Center, Hiroshima University, Higashi-Hiroshima, Hiroshima 739-8526, Japan
[49] Vatican Observatory, Castel Gandolfo, V-00120, Vatican City State
[50] Istituto Nazionale di Fisica Nucleare, Sezione di Trieste, and Università di Trieste, I-34127 Trieste, Italy
[51] Department of Physics and Astronomy, University of Denver, Denver, CO 80208, USA
[52] Instituto Nacional de Astrofísica, Óptica y Electrónica, Tonantzintla, Puebla 72840, Mexico
[53] Istituto Nazionale di Astrofisica-Osservatorio Astrofisico di Torino, via Osservatorio 20, I-10025 Pino Torinese, Italy
[54] East Asian Observatory, Hilo, HI 96720, USA
[55] Osservatorio Astronomico di Trieste, Istituto Nazionale di Astrofisica, I-34143 Trieste, Italy
[56] Korea Astronomy and Space Science Institute, 776 Daedeokdae-ro, Yuseong-gu, Daejeon 30455, Republic of Korea
[57] Department of Physics, American University, Washington, DC 20016, USA
[58] Centre for Astro-Particle Physics (CAPP) and Department of Physics, University of Johannesburg, PO Box 524, Auckland Park 2006, South Africa
[59] Laboratoire Univers et Particules de Montpellier, Université Montpellier, CNRS/IN2P3, F-34095 Montpellier, France
[60] NYCB Real-Time Computing Inc., Lattingtown, NY 11560-1025, USA
[61] Purdue University Northwest, Hammond, IN 46323, USA
[62] Solar-Terrestrial Environment Laboratory, Nagoya University, Nagoya 464-8601, Japan
[63] Institute of Space Sciences (ICE, CSIC), Campus UAB, Carrer de Magrans s/n, E-08193 Barcelona, Spain
[64] Institut d'Estudis Espacials de Catalunya (IEEC), E-08034 Barcelona, Spain
[65] Institució Catalana de Recerca i Estudis Avançats (ICREA), E-08010 Barcelona, Spain
[66] Centre for Space Research, North-West University, Potchefstroom Campus, Private Bag X6001, Potchefstroom 2520, South Africa
[67] Center for Astrophysics and Cosmology, University of Nova Gorica, Nova Gorica, Slovenia
Received 2022 June 17; revised 2022 September 14; accepted 2022 September 23; published 2022 November 16

Abstract

An incremental version of the fourth catalog of active galactic nuclei (AGNs) detected by the Fermi Large Area Telescope is presented. This version (4LAC-DR3) derives from the third data release of the 4FGL catalog based on 12 yr of $E > 50$ MeV gamma-ray data, where the spectral parameters, spectral energy distributions (SEDs), yearly light curves, and associations have been updated for all sources. The new reported AGNs include 587 blazar candidates and four radio galaxies. We describe the properties of the new sample and outline changes affecting the previously published one. We also introduce two new parameters in this release, namely the peak energy of the SED high-energy component and the corresponding flux. These parameters allow an assessment of the Compton dominance, the ratio of the inverse-Compton to the synchrotron-peak luminosities, without relying on X-ray data.

Unified Astronomy Thesaurus concepts: Active galactic nuclei (16); Gamma-ray astronomy (628); Blazars (164); Flat-spectrum radio quasars (2163); BL Lacertae objects (158); Spectral energy distribution (2129)

Supporting material: machine-readable table

1. Introduction

Since its launch in 2008, the Fermi Large Area Telescope (LAT; Atwood et al. 2009) has enabled the discovery of new classes of gamma-ray emitters and the detection of much larger and better-characterized source populations than previously achieved. Active galactic nuclei (AGNs) represent by far the most abundant source population of the LAT detected sources. The 4LAC catalog (4LAC-DR1; Ajello et al. 2020), based on the 4FGL source catalog (4FGL-DR1; Abdollahi et al. 2020) established with 8 yr of data, comprised 2863 $|b| > 10^{\circ}$ AGNs while 344 others were found at lower latitudes. As more data accumulate, the catalogs are regularly updated. Updates of 4FGL use the same data version ("P8R3") and Galactic diffuse emission model as the initial catalog. Sources previously reported are kept in even if they fall below the TS = 25 threshold over the extended period of data taking. These sources retain their original positions, in contrast to new catalogs where all positions are reevaluated and subthreshold sources are omitted. The second data releases, 4FGL-DR2 (Ballet et al. 2020) and 4LAC-DR2 (comprising 285 new AGNs; Lott et al. 2020), were based on 10 yr of data.

Here we present the third update to the 4LAC catalog, derived from 4FGL-DR3 (Abdollahi et al. 2022) using 12 yr of data and comprising 1607 new sources relative to the initial 4FGL catalog. The properties of the 283 new 4FGL-DR2[69] and 308 new 4FGL-DR3 AGNs (DR2 and DR3 tallies will be aggregated in the following) are discussed. These AGNs are all blazars except for four radio galaxies. Besides providing a larger AGN sample for population studies, releasing periodic updates to 4LAC offers new targets for programs dedicated to classifying LAT blazars or measuring redshifts as detections come along (e.g., Desai et al. 2019; Peña-Herazo et al. 2020, 2021a, 2021b; Peña-Herazo et al. 2021c; Goldoni et al. 2021; Rajagopal et al. 2021).

The paper is organized as follows. Section 2 summarizes the analysis improvements introduced in 4FGL-DR3. Changes affecting 4LAC-DR1 AGNs are listed in Section 3. Section 4 presents the new DR3 sources, while Section 5 discusses the peak energy of the spectral energy distributions (SED) high-energy component, estimated from the spectral curvature, and the derived Compton dominance. A summary closes the paper in Section 6.

2. Analysis Improvements—Source Associations

We refer the reader to the 4FGL-DR3 paper (Abdollahi et al. 2022) for details on the gamma-ray data analysis. The methodology that was followed is essentially the same as that pursued in the 4FGL-DR1 catalog. The first stage includes the detection

[68] NASA Postdoctoral Program Fellow.

[69] Two AGNs first reported in DR2 are missing in DR3 because the gamma-ray sources (4FGL J1242.4−2948 and 4FGL J1752.2−3002) have been either relocalised or deleted (being exceptions to the rule stated above).

and localization of the sources. The second one comprises thresholding, spectral characterization, and production of light curves. The same flags as in 4FGL-DR1 are then generated. They indicate the limited robustness of the results against different analysis ingredients or a warning about particular source conditions (e.g., proximity to a bright source). The association with counterparts known at other wavelengths constitutes the final stage of the analysis.

The (nonexhaustive) list of changes relative to 4FGL-DR1[70] is as follows. An updated version of the instrument-response functions (P8R3_SOURCE_V3) has been used. The analysis weights have been recalculated. These weights downplay the contribution of low-energy, low-latitude photons to the likelihood in order to reduce the associated systematic uncertainties. The handling of the energy dispersion has been improved. Bayesian priors have been applied when fitting the parameters of the diffuse emission model in each region of interest to hinder their excursion relative to their expected values (normalization = 1, photon-index correction = 0). The threshold for considering spectral curvature as significant has been lowered from 3σ to 2σ, leading to an increase of the fraction of curved sources from 30% in 4FGL-DR1 to 54% in 4FGL-DR3. This change has removed unphysical upturns in the global source spectrum at low (<200 MeV) and high (>20 GeV) energy. It has important implications for the characterization of the LAT blazars since the peak energy of the SED high-energy component (referred to as the inverse-Compton component in the following, assuming that relativistic electrons are the main emitting particles) and its flux can be derived from the fitted log parabola. The number of bins in the SED has been increased from seven to eight. The yearly light curves have been updated (while the two-monthly ones reported in 4FGL-DR1 have not). Specific to the 4LAC update, the highest photon energy detected for each source has been updated. The information about the highest detected energy is particularly relevant for studies of the extragalactic background light (e.g., Saldana-Lopez et al. 2021).

The association procedure makes use of two different methods, the Bayesian method (Abdo et al. 2010b) and the likelihood-ratio method (LR; Ackermann et al. 2011, 2015), which are both based on spatial coincidence. The main change in seeking counterparts concerns the use of an updated version of the radio fundamental catalog.[71] Only associations with a probability of being real greater than 0.8 in either association method are retained. For the 591 new AGNs, 253 are associated solely with the Bayesian method, 65 solely with the LR method, and 273 with both methods.

The same classification scheme as in the 4LAC-DR1 catalog has been followed. An optical class in terms of a flat spectrum radio quasar (FSRQ) and BL Lacertae (BL Lac)-type object, assessed according to the strength of the optical emission lines, is provided if spectroscopic data of sufficiently good quality are found in the literature. An SED-based class is derived from the value of the peak frequency ($\nu_{\rm pk}^{\rm syn}$) of the synchrotron component fitted to archival data using the SED data archive and SED(t)-Builder interactive web tool available at the Italian Space Agency (ASI) Space Science Data Center (SSDC).[72] The class can be a low-synchrotron-peaked blazar (LSP; for sources with $\nu_{\rm pk}^{\rm syn} < 10^{14}$ Hz), an intermediate-synchrotron-peaked blazar (ISP; for $10^{14}\,{\rm Hz} < \nu_{\rm pk}^{\rm syn} < 10^{15}$ Hz), or a high-synchrotron-peaked blazar (HSP; if $\nu_{\rm pk}^{\rm syn} > 10^{15}$ Hz). SED-based classification is missing for 139 new AGNs, mainly because of a lack of broadband data.

3. Changes to 4LAC-DR1

For completeness, we reiterate here the changes to 4LAC-DR1 AGNs as outlined in the 4FGL-DR2 document (Lott et al. 2020). About 200 counterpart names of DR1 sources have been changed. It was noted that blazar names from very large surveys (such as the Two Micron All Sky Survey; 2MASS, or the Wise-field Infrared Survey Explorer; WISE) were used for some 4FGL associations while more common names from radio catalogs were available. Moreover some names referred to sources that are offset by up to a few arcminutes from the real counterpart. We have replaced the nonradio names with those of radio counterparts whenever possible. Note that the positions reported in the 4FGL-DR1 (`RA_Counterpart`, `DEC_Counterpart`) fields were correct.

Changes in associations of 4LAC-DR1 sources are listed below.

1. Recent follow-up observations of 4FGL blazars (e.g., Peña-Herazo et al. 2017; Desai et al. 2019; Peña-Herazo et al. 2019; Peña-Herazo et al. 2020, 2021a, 2021b; Peña-Herazo et al. 2021c; Rajagopal et al. 2021) have enabled the classification of 240 former blazar candidates of unknown types (BCUs), two AGNs, and two unknowns (UNKs)[73] into 214 BL Lac objects and 30 FSRQs. In particular, Paliya et al. (2020a) found that the former BCU associated with 4FGL J1219.0+3653 is a BL Lac object with a redshift of 3.53, making it the most distant BL Lac object detected by the LAT.
2. The latest version of the radio fundamental catalog has enabled the association with blazar candidates of six previously unassociated sources and two SPPs (SPPs designate potential associations with supernova remnants or pulsar-wind nebulae). These sources are 4FGL J0129.0+6312 (2MASS J01283059+6306298), 4FGL J0550.9+2552 (NVSS J055119+254909), 4FGL J0803.5+2046 (GB6 B0800+2046), 4FGL J1102.0−6054 (2MASS J11015838−6056516), 4FGL J1347.4+7309 (NVSS J134734+731812), 4FGL J1606.6+1324 (NVSS J160654+131934), 4FGL J1738.0+0236 (PKS 1735+026), and 4FGL J2249.9+0452 (WISEA J225007.35+045617.3).
3. Three sources (TXS 0159+085, PKS 0736−770, and TXS 1530−131) were incorrectly classified as FSRQs. They have been reclassified as BCUs. Two other FSRQs (RX J0134.4+2638 and 2MASS J02212698+2514338) have been reclassified as BL Lac objects.[74]
4. Following Järvelä et al. (2020), we have reclassified TXS 2116−077 (4FGL J2118.8−0723) as a Seyfert galaxy instead of a NLSY1 (see Paliya et al. 2020b, for an alternative view).
5. The tentative association of 4FGL J0647.7−4418 with the high-mass X-ray binary RX J0648.0−4418 reported in 4FGL-DR1 has been replaced by the association with

[70] DR2 was produced with only minor analysis changes relative to DR1.
[71] rfc_2021a available at http://astrogeo.org/rfc/.
[72] http://tools.ssdc.asi.it/SED/
[73] The UNK class corresponds to $|b| < 10°$ sources solely associated with the LR method, which may suffer from contamination with Galactic sources.
[74] TXS 0159+085 and RX J0134.4+2638 were still classified as FSRQs in 4FGL-DR3.

the BCU SUMSS J064744−441946 following the multiwavelength investigation of Martí et al. (2020).

A total of 214 additional 4LAC-DR1 sources are now classified as variable thanks to the extended yearly light curves produced in DR3. These sources comprise 26 FSRQs, 105 BL Lac objects, 80 BCUs, and three radio galaxies (IC 1531, PKS 0625−35, and Cen A). Concerning the iconic radio galaxy Cen A, its flux dropped significantly (14%) in the last 4 yr spanned by this release.

Photons with higher energies than previously detected in the earlier 8 yr have been found for 471 4FGL-DR1 sources during the additional 4 yr of data taking. Only $E > 10$ GeV, ULTRACLEAN_VETO photons with a probability greater than 0.95 to belong to the source have been considered.

4. The 4LAC-DR3 and Low-latitude Samples

The 4LAC-DR3 sample comprises AGNs located at $|b| > 10°$, in keeping with the 4LAC defining criterion. The same defining criterion for the clean sample (i.e., sources with no analysis flags) as in 4LAC-DR1 has been used in this paper. The AGNs lying at $|b| < 10°$ constitute the low-latitude sample.[75] Table A1 describes the format of the catalog FITS files.

The new AGNs relative to 4LAC-DR1 include 587 blazars: 75 FSRQs, 117 BL Lac objects, 395 BCUs, and four radio galaxies (eight BCUs have been classified into seven BL Lac objects and one FSRQ since the DR2 release). The 4LAC-DR3 comprises 542 ($|b| > 10°$) new AGNs. While FSRQs are almost evenly distributed between the northern and southern Galactic hemispheres (40 and 35, respectively), a strong deficit is observed in the south for BL Lac objects (80 versus 37), while the opposite trend is seen for BCUs (166 versus 229). These imbalances are probably due to fewer programs observing the southern region. The low-latitude sample includes 49 sources (all BCUs except for one BL Lac object).

Table 1 gives the census of the new AGNs, while Table 2 provides that of the whole population. Figures 1 and 2 compare the photon-index and redshift distributions, respectively, between the new and 4LAC-DR1 samples for different blazar classes.

The median photon index of the new FSRQs is larger (2.61 versus 2.45) than that of the DR1 sample, indicating softer spectra. The median redshift is similar to 4LAC-DR1 (1.19 versus 1.12). PKS 2318−087 (4FGL J2320.8−0823) with $z = 3.164$ has the highest redshift of the new 4LAC-DR3 FSRQs, though four 4LAC-DR1 FSRQs have higher redshifts (up to 4.31). A total of 32 new FSRQs (seven of them with TS > 100) are found to be variable and 12 of them, which are more significant than average, show pronounced flares in the last 4 yr of the 12 yr period.

Of the 117 new BL Lac objects, an SED-based classification could be obtained for 94 of them, comprising 22 LSPs, 27 ISPs, and 46 HSPs. The new BL Lac objects have a median photon index similar to the DR1 ones (2.00 versus 2.03). The median redshift of the 78 BL Lac objects with measured values is 0.28, which is comparable to that of 4LAC-DR1 (0.34). The maximum redshift is 0.848 for RX J1438.3+1204 (4FGL J1438.6+1205), while the maximum redshift of 4LAC-DR1 BL Lac objects is 3.53. Only six new BL Lac objects (all with TS < 100) are found to be variable.

BCUs represent more than two thirds of the new blazars due to a lack of reliable spectroscopic data. Some insight into the nature of these sources can nevertheless be gained by inspecting their photon-index distributions, building on the remarkably distinct distributions exhibited by FSRQs and BL Lac objects. The BCU distribution, with a median photon index notably higher than the corresponding DR1 value (i.e., 2.36 and 2.23, respectively), is compared to the (normalized)

Table 1
Census of New DR2-DR3 Sources

AGN Type	High-latitude Sample	Clean Sample[a]	Low-latitude Sample
All	542	430	49
FSRQ	75	56	0
…LSP	67	49	0
…ISP	5	5	0
…HSP	1	1	0
…no SED classification	2	1	0
BL Lac Object	116	97	1
…LSP	22	20	1
…ISP	27	19	0
…HSP	46	40	0
…no SED classification	21	18	0
Blazar of Unknown Type	347	273	48
…LSP	172	130	26
…ISP	35	29	4
…HSP	41	38	1
…no SED classification	99	76	17
Nonblazar AGN	4	4	0
…radio galaxies	4	4	0

Note.
[a] Sources in the high-latitude sample without analysis flags.

Table 2
Census of 4LAC-DR3 Sources

AGN Type	High-latitude Sample	Clean Sample[a]	Low-latitude Sample
All	3407	2896	407
FSRQ	755	640	37
…LSP	672	581	35
…ISP	20	18	0
…HSP	4	4	0
…no SED classification	59	37	2
BL Lac Object	1379	1261	79
…LSP	353	332	20
…ISP	347	309	8
…HSP	425	394	29
…no SED classification	254	226	22
Blazar of Unknown Type	1208	945	285
…LSP	508	397	78
…ISP	135	115	12
…HSP	117	99	10
…no SED classification	448	334	185
Nonblazar AGN	65	50	6
…radio galaxies	42	32	4

Note.
[a] Sources in the high-latitude sample without analysis flags.

[75] The 4LAC-DR3 and low-latitude files are available at https://fermi.gsfc.nasa.gov/ssc/data/access/lat/4LACDR3/table-4LAC-DR3-h.fits and https://fermi.gsfc.nasa.gov/ssc/data/access/lat/4LACDR3/table-4LAC-DR3-l.fits, respectively.

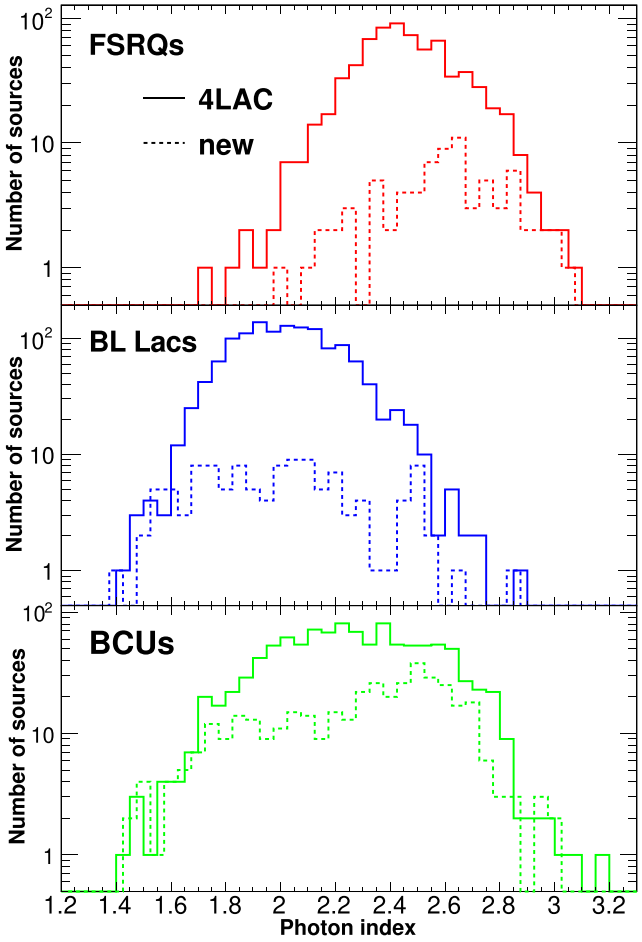

Figure 1. Comparison between the photon-index distributions of 4LAC-DR1 and new (DR2 and DR3) blazars for different classes.

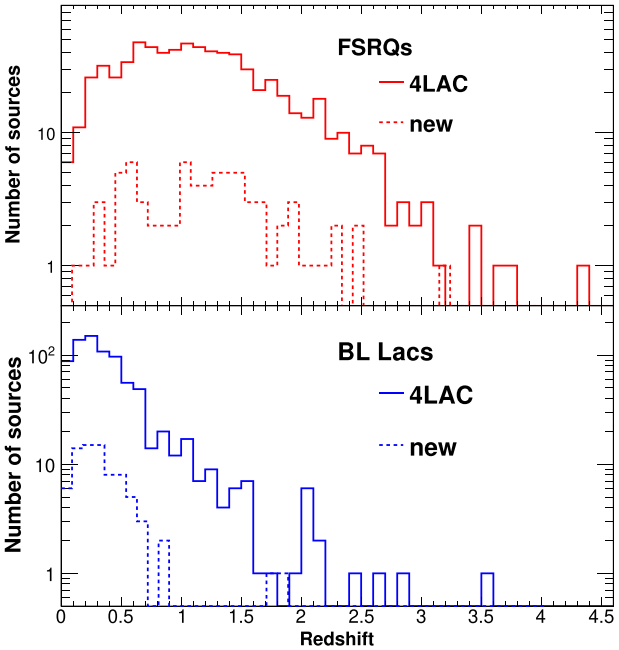

Figure 2. Comparison between the redshift distributions of 4LAC-DR1 and new (DR2 and DR3) blazars for different classes.

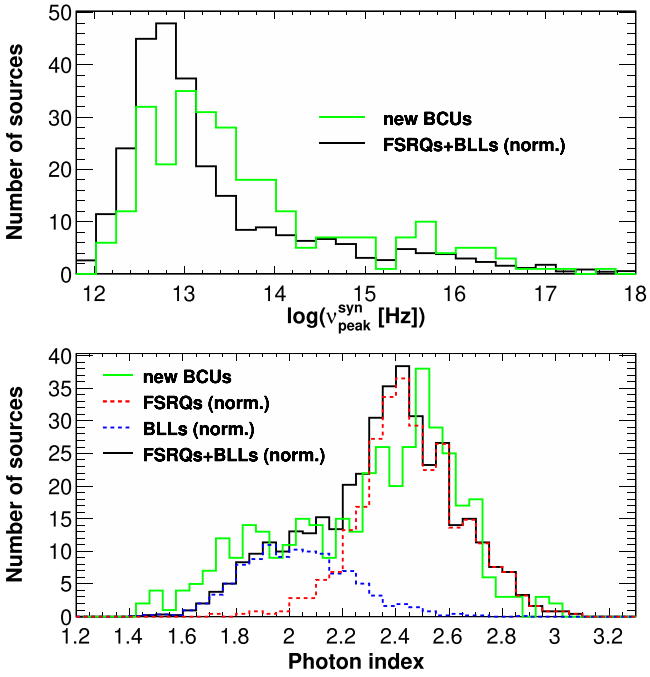

Figure 3. Distributions of $\nu_{\rm pk}^{\rm syn}$ (top) and photon index (bottom) of the new (DR2 and DR3) BCUs (green, solid) compared to the arbitrarily normalized sum of the FSRQ and BL Lac object distributions (solid, black). The relative weight between FSRQs and BL Lac objects has been multiplied by 2.5 with respect to that found in 4FGL.

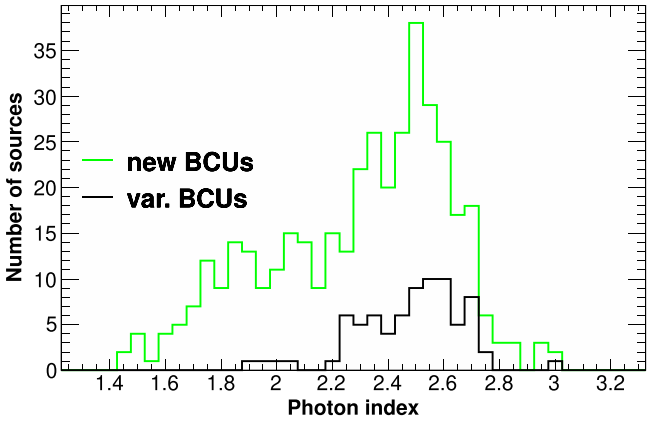

Figure 4. Photon-index distributions for the new BCUs and the subset of sources showing significant variability.

FSRQ and BL Lac object distributions in Figure 3. To best reproduce the BCU distribution with a linear combination of the latter distributions, the relative weight of FSRQs must be increased by a factor $\simeq$2.5 with respect to that found in the 4LAC-DR3 sample. In 4LAC-DR1, the BCU distribution could be well reproduced by assuming the same fractions of FSRQs and BL Lac objects as found in the classified population (see Figure 6 in Ajello et al. 2020). This excess of new FSRQ candidates in 4LAC-DR3 may come from the stronger flaring activity of FSRQs relative to BL Lac objects in the LAT energy range. The photon-index distribution of the 77 variable BCUs, with 15 of them having TS $>$ 100, supports this idea (Figure 4). The observation of slightly softer spectra relative to the bulk of FSRQs for both the new FSRQ-like BCUs and the new FSRQs is compatible with this explanation. This effect holds for sources of both classes with detected variability. Out of the 396

new BCUs, only seven have measured redshifts. These have photon indices similar to those of FSRQs. This observation applies to the whole population of BCUs with measured redshifts.

The four new radio galaxies are NGC 3078, NGC 4261, LEDA 55267, and NGC 6454. NGC 3078 is a nearby (d=35 Mpc) compact-core-dominated galaxy (Wrobel & Heeschen 1984). NGC 4261 ($d = 30$ Mpc) is a LINER Fanaroff–Riley type I (FR I) radio galaxy, whose LAT detection was first reported by de Menezes et al. (2020). The detection of LEDA 55267 was first reported by Paliya (2021). It was classified there as a Fanaroff–Riley type 0 radio galaxy, i.e., having similar nuclear and host properties as FR I's but significantly fainter extended radio emission (Grandi et al. 2016). NGC 6454 is an FR I galaxy (Britzen et al. 2008; van Velzen et al. 2012) at a distance of 130 Mpc.[76]

5. Peak Energy of the High-energy Component—Compton Dominance

Two new parameters are provided in the DR3 release for the whole set of LAT blazars: the peak energy ($E_{\rm pk}^{\rm IC}$), or equivalently the peak frequency ($\nu_{\rm pk}^{\rm IC}$), and the corresponding flux ($\nu F_\nu^{\rm IC}$) of the SED high-energy component in the observer frame. Thanks to the improved statistics and the relaxed threshold for considering spectral curvature as significant, 1601 LAT blazars have a significantly curved spectrum, from which these two parameters can be estimated using a fit of a log normal function. This assessment of $E_{\rm pk}^{\rm IC}$ is an alternative to that based on a polynomial fit to the IC component using both X-ray and gamma-ray data (e.g., as in Abdo et al. 2010a). The latter assessment may suffer from the fact that multiple processes can contribute to the IC component, making its actual shape uncertain. Here we restrict the discussion to sources with a relative uncertainty on $E_{\rm pk}^{\rm IC}$ lower than 50%. This condition favors sources with slightly harder gamma-ray spectra than average. The effect is more pronounced for FSRQs (mean photon-index difference relative to the whole sample: $\Delta\Gamma = 0.08$), and diminishes for BL Lac objects as $\nu_{\rm pk}^{\rm syn}$ increases (from $\Delta\Gamma = 0.05$ for LSPs to $\Delta\Gamma = 0.03$ for HSPs). Overall, the fraction of sources with $E_{\rm pk}^{\rm IC}$ meeting the above condition is 30%, 28%, and 24% for FSRQS, BL Lac objects, and BCUs, respectively. FSRQs preferentially exhibit $E_{\rm pk}^{\rm IC}$ below 1 GeV, while most BL Lac objects have $E_{\rm pk}^{\rm IC}$ above this value, reflecting the dichotomy seen in the photon-index distributions (Figure 1). Most values of $E_{\rm pk}^{\rm IC}$ obtained for the nine radio galaxies meeting the above condition are notably larger than those reported from a combined fit to the X-ray and gamma-ray data (see, e.g., Fukazawa et al. 2022). An explanation for this discrepancy can be the presence of a prominent emission from the corona/accretion disk in the X-ray to soft gamma-ray bands, which drives down the fitted $E_{\rm pk}^{\rm IC}$ value in the latter case.

Except in very rare cases (five sources), $E_{\rm pk}^{\rm IC}$ lies within the Fermi-LAT energy range ($E_{\rm pk} > 50$ MeV) and is thus reasonably well constrained on the lower-energy side. In the following, we apply no corrections for the extinction due to the extragalactic background light, which affects E > 10 GeV photons. Reported values of $E_{\rm pk}^{\rm IC}$ greater than 10 GeV must thus be considered as lower limits, as must the associated $\nu F_\nu^{\rm IC}$ values. Figure 5 displays $\nu F_\nu^{\rm IC}$ as a function of $E_{\rm pk}^{\rm IC}$. An estimated threshold for determining the two parameters with the required significance/accuracy is plotted in this Figure. This threshold was calculated as a polynomial fit to the data of blazars with $\Delta E_{\rm pk}^{\rm IC} = (50 \pm 5)\%$.

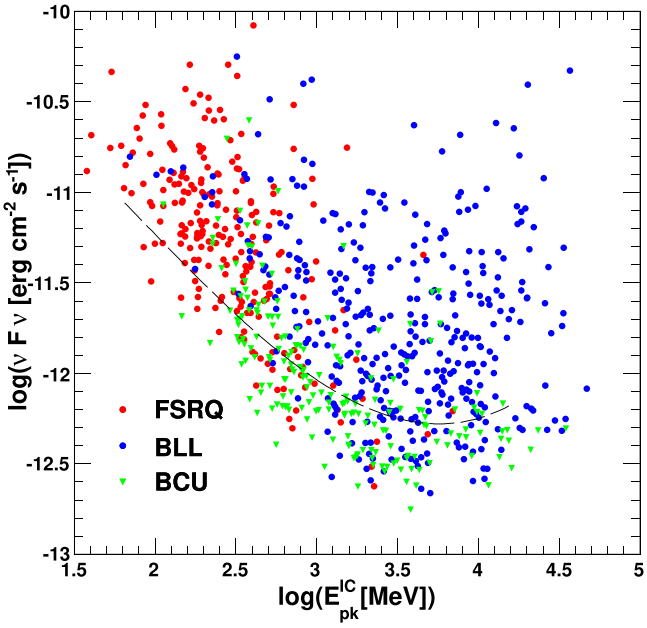

Figure 5. $\nu F\nu$ of the high-energy peak as a function of the peak energy for sources fulfilling the conditions given in the text. Error bars have been omitted for clarity. The dashed curve corresponds to an estimated average threshold.

A detailed study of blazar populations is beyond the scope of this paper so we just outline some broad features. The synchrotron-peak frequency could be determined for 785 of these blazars, including 230 FSRQs, 362 BL Lac objects, and 193 BCUs. In a simple single-zone synchrotron self-Compton model and assuming inverse-Compton scattering in the Thomson regime, the peak Lorentz factor of the electron distribution $\gamma_{\rm SSC^{pk}}$ most contributing to the electromagnetic emission can be directly assessed in a redshift-independent way from the two peak frequencies $\gamma_{\rm pk}^{\rm SSC} = \left(\frac{3\,\nu_{\rm pk}^{\rm IC}}{4\,\nu_{\rm pk}^{\rm syn}}\right)^{1/2}$. These frequencies, evaluated in the source rest frame[77], are plotted as a function of one another in Figure 6. We emphasize that the estimates of $\nu_{\rm pk}^{\prime\rm syn}$ and $E_{\rm pk}^{\prime\rm IC}$ are obtained independently, so near-empty regions in Figure 6 do not result from an observational or analysis bias. BCUs follow the same general trend seen for FSRQs and BL Lac objects.

The correlation between $\nu_{\rm pk}^{\prime\rm syn}$ and $E_{\rm pk}^{\prime\rm IC}$ is strong for BL Lac objects (Pearson coefficient = 0.75) but weak for FSRQs (Pearson coefficient = 0.08 for $\log(\nu_{\rm pk}^{\prime\rm syn}) < 13.6$, comprising 90% of the sample). A fit of a linear function

$$\log(E_{\rm pk}^{\prime\rm IC}) = \alpha \times \log(\nu_{\rm pk}^{\prime\rm syn}) + K \quad (1)$$

(with $E_{\rm pk}^{\prime\rm IC}$ in MeV and $\nu_{\rm pk}^{\prime\rm syn}$ in hertz) to the BL Lac object data provides $\alpha = 0.366$ and $K = -1.71$. A similar fit for the

[76] This source was classified as an "AGN" in 4FGL-DR3.

[77] Primed quantities are evaluated in the source rest frame. For BL Lac objects and BCUs without measured redshifts, values of $z = 0.38$ and 0.56, corresponding to the median measured redshifts for these two classes, have been assumed, respectively.

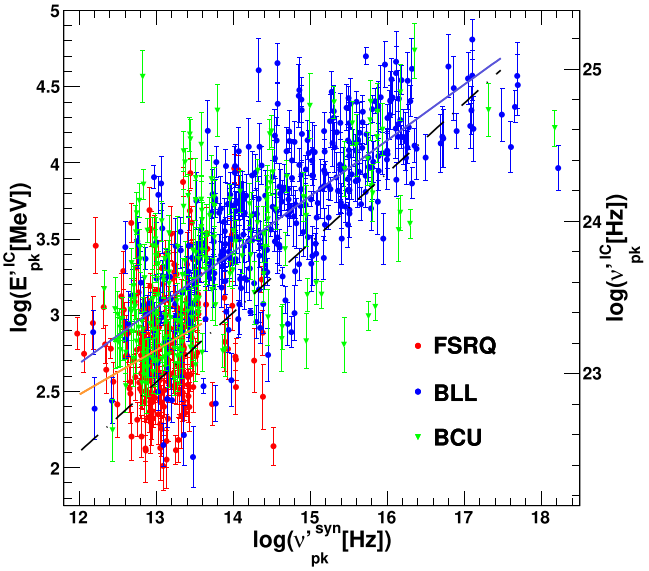

Figure 6. Energy of the high-energy component plotted as a function of $\nu'^{\rm syn}_{\rm pk}$, both estimated in the rest frame, for the different blazar classes. The source selection is described in the text. The blue line represents a linear fit to the BL Lac object data and the orange one (restricted to $\log(\nu'^{\rm syn}_{\rm pk}) < 13.6$) to the FSRQ data. The black dashed–dotted line corresponds to the prescription from Abdo et al. (2010a).

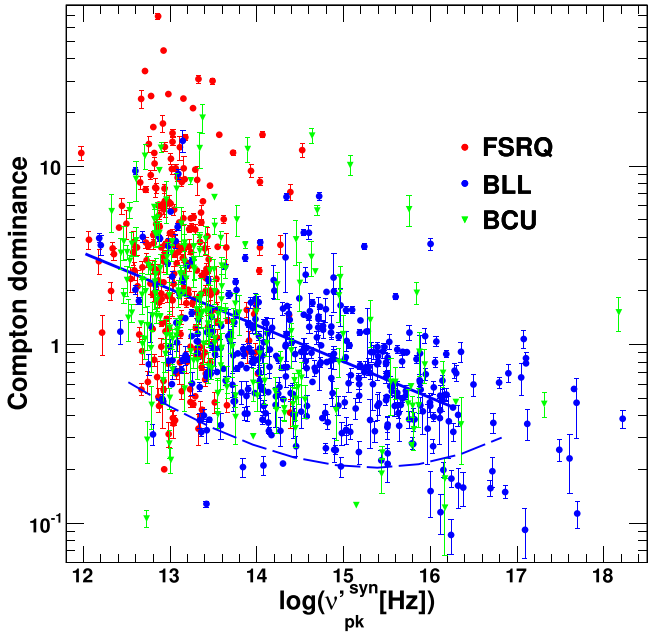

Figure 7. Compton dominance plotted as a function of $\nu'^{\rm syn}_{\rm pk}$ for the same sources as in Figure 6. The dashed line corresponds to an estimate of the average threshold for BL Lac objects (derived from the threshold plotted in Figure 5) and the solid line to an exponential fit to the BL Lac object data.

FSRQs[78] restricted to $\log(\nu'^{\rm syn}_{\rm pk}) < 13.6$ yields $\alpha = 0.293$ and $K = -1.03$. The trend obtained from Equation (5) in Abdo et al. (2010a) (derived using broadband data from 48 bright blazars including 23 FSRQs, 23 BL Lac objects, and two BCUs) is also shown in Figure 6.

The Compton dominance is defined as the ratio between the peak νF_ν for the high- and low-frequency SED components. This redshift-independent parameter has been intensively discussed in the context of the blazar sequence (e.g., Meyer et al. 2011; Finke 2013; Nalewajko & Gupta 2017; Paliya et al. 2021). The Compton dominance is plotted as a function of $\nu'^{\rm syn}_{\rm pk}$ in Figure 7, together with the threshold derived from that plotted in Figure 5. The trend is very similar to that seen when the Compton dominance is assessed using the prescription of Abdo et al. (2010a). Fitting the BLLac object (log–log) data in Figure 7 with a linear function gives a slope of -0.46 ± 0.12. No clear indication of an upturn around $\nu_{\rm pk} \simeq 10^{14}$ Hz manifesting the transition between synchrotron self-Compton and external Compton as the dominant emission process (Finke 2013) is seen in Figure 7. However, the larger scatter in Compton dominance observed for FSRQs relative to BL Lac objects is likely due to this difference in main emission processes (external-Compton versus synchrotron self-Compton), in addition to different variability levels.

6. Summary

The new release (4FGL-DR3) includes about 19% more blazars than the initial 4LAC-DR1, comprising 75 FSRQs, 117 BL Lac objects, 395 BCUs, and four radio galaxies. The large fraction of BCUs (two thirds) calls for new spectroscopic data to enable the classification. The BCU photon-index distribution suggests that the fraction of FSRQs within these BCUs is notably larger (by a factor $\simeq$2.5) than that found in the set of classified blazars. This feature, not apparent in 4LAC-DR1, may result from a larger flaring propensity of FSRQs relative to BL Lac objects in the LAT energy range, as exemplified, e.g., by the very different fractions (42% versus 6%) of variable 4FGL-DR3 sources seen in these classes. Both redshift and photon-index distributions of the new FSRQs and BL Lac objects are similar to the previously detected ones. Thanks to the new data and a looser threshold regarding variability, 214 additional 4FGL-DR1 sources are now considered variable. A total of 1602 LAT blazars have a significantly curved spectrum, from which the peak position of the high-energy SED component and its corresponding flux can be estimated from the gamma-ray data alone by fitting a log normal function. These parameters combined with the position of the synchrotron peak estimated from archival data allows us to derive the Compton dominance.

The Fermi LAT Collaboration acknowledges generous ongoing support from a number of agencies and institutes that have supported both the development and the operation of the LAT as well as scientific data analysis. These include the National Aeronautics and Space Administration and the Department of Energy in the United States, the Commissariat à l'Energie Atomique and the Centre National de la Recherche Scientifique / Institut National de Physique Nucléaire et de Physique des Particules in France, the Agenzia Spaziale Italiana and the Istituto Nazionale di Fisica Nucleare in Italy under ASI-INFN Agreements No. 2021-43-HH.0, the Ministry of Education, Culture, Sports, Science and Technology (MEXT), High Energy Accelerator Research Organization (KEK) and Japan Aerospace Exploration Agency (JAXA) in Japan, and the K. A. Wallenberg Foundation, the Swedish Research Council and the Swedish National Space Board in Sweden. Additional support for science analysis during the operations phase is gratefully acknowledged from the Istituto Nazionale di

[78] Fitting the peak positions in the observer frame yields $\alpha = 0.374$ (0.344) and $K = -1.92$ (-1.93) for BL Lac objects (FSRQs).

Astrofisica in Italy and the Centre National d'Études Spatiales in France. This work performed in part under DOE Contract DE-AC02-76SF00515.

This research has made use of the NASA/IPAC Extragalactic Database (NED) (2019), which is operated by the Jet Propulsion Laboratory, California Institute of Technology, under contract with the National Aeronautics and Space Administration, and of archival data, software, and online services provided by the ASI Space Science Data Center (SSDC) operated by the Italian Space Agency. D.Ga. and S.Ci. acknowledge support by ASI through contract ASI-INFN 2021-43-HH.0 for SSDC, and the Istituto Nazionale di Fisica Nucleare (INFN)

Appendix
Description of the FITS Version of the 4LAC-DR3 Catalog

Table A1 provides a description of the FITS catalogs available in the online journal. There are separate FITS catalogs for the (high-latitude) 4LAC-DR3 and low-latitude sources.

Table A1
4LAC-DR3 FITS Format

Column	Format	Unit	Description
Source_Name	18A	⋯	Source name 4FGL JHHMM.m+DDMMa[a]
DataRelease	I		1 for 4FGL, 2 for new in DR2, 3 for new or changed in DR
RAJ2000	E	deg	R.A.
DEJ2000	E	deg	Decl.
GLON	E	deg	Galactic longitude
GLAT	E	deg	Galactic latitude
Signif_Avg	E	⋯	Source significance in σ units over the 50 MeV to 1 TeV band
Flux1000	E	cm^{-2} s^{-1}	Integral photon flux from 1 to 100 GeV
Unc_Flux1000	E	cm^{-2} s^{-1}	1σ error on integral photon flux from 1 to 100 GeV
Energy_Flux100	E	erg cm^{-2} s^{-1}	Energy flux from 100 MeV to 100 GeV obtained by spectral fitting
Unc_Energy_Flux100	E	erg cm^{-2} s^{-1}	1σ error on energy flux from 100 MeV to 100 GeV
SpectrumType	17A	⋯	Spectral type in the global model (PowerLaw, LogParabola, PLSuperExpCutoff)
PL_Index	E	⋯	Photon index when fitting with PowerLaw
Unc_PL_Index	E	⋯	1σ error on PL_Index
Pivot_Energy	E	MeV	Pivot energy
LP_Index	E	⋯	Photon index at Pivot_Energy (α) when fitting with LogParabola
Unc_LP_Index	E	⋯	1σ error on LP_Index
LP_beta	E	⋯	Curvature parameter (β) when fitting with LogParabola
Unc_LP_beta	E	⋯	1σ error on LP_beta
Flags	I	⋯	Analysis flags
CLASS	6A	⋯	Class designation for associated source
ASSOC1	30A	⋯	Name of identified or likely associated source
ASSOC_PROB_BAY	E	⋯	Probability of association according to the Bayesian method
ASSOC_PROB_LR	E	⋯	Probability of association according to the likelihood-ratio method
Counterpart_Catalog	10A		Counterpart catalog driving the association
RA_Counterpart	D	deg	R.A. of the counterpart ASSOC1
DEC_Counterpart	D	deg	Decl. of the counterpart ASSOC1
Unc_Counterpart	E	deg	95% precision of the counterpart localization
VLBI_Counterpart	14A	⋯	Name of the very long baseline interferometry counterpart
Redshift	E	⋯	Redshift
SED_class	6A	⋯	SED-based class
HE_EPeak	E	MeV	Energy in the observer frame of the high-energy SED peak
Unc_HE_EPeak	E	MeV	1σ error on energy of the high-energy SED peak
HE_nuFnuPeak	E	erg cm^{-2} s^{-1}	$\nu F\nu$ at high-energy-peak frequency
Unc_HE_nuFnuPeak	E	erg cm^{-2} s^{-1}	1σ error on spectral energy distribution at high-energy-peak frequency
nu_syn	E	Hz	Synchrotron-peak frequency in the observer frame
nuFnu_syn	E	erg cm^{-2} s^{-1}	$\nu F\nu$ at synchrotron-peak frequency
Variability_Index	E	⋯	Variability index
Frac_Variability	E	⋯	Fractional variability
Unc_Frac_Variability	E	⋯	1σ error on fractional variability
Highest_energy	E	GeV	Energy (if greater than 10 GeV) of the highest-energy ULTRACLEANVETO photon with association probability $P > 0.95$

Note.
[a] The coordinates are rounded, following the International Astronomical Union convention.

(This table is available in its entirety in machine-readable form.)

ORCID iDs

M. Ajello https://orcid.org/0000-0002-6584-1703
L. Baldini https://orcid.org/0000-0002-9785-7726
J. Ballet https://orcid.org/0000-0002-8784-2977
D. Bastieri https://orcid.org/0000-0002-6954-8862
J. Becerra Gonzalez https://orcid.org/0000-0002-6729-9022
R. Bellazzini https://orcid.org/0000-0002-2469-7063
E. Bissaldi https://orcid.org/0000-0001-9935-8106
R. Bonino https://orcid.org/0000-0002-4264-1215
A. Brill https://orcid.org/0000-0002-6208-5244
P. Bruel https://orcid.org/0000-0002-9032-7941
S. Buson https://orcid.org/0000-0002-3308-324X
R. Caputo https://orcid.org/0000-0002-9280-836X
P. A. Caraveo https://orcid.org/0000-0003-2478-8018
C. C. Cheung https://orcid.org/0000-0002-4377-0174
N. Cibrario https://orcid.org/0000-0003-3842-4493
S. Ciprini https://orcid.org/0000-0002-0712-2479
F. D'Ammando https://orcid.org/0000-0001-7618-7527
N. Di Lalla https://orcid.org/0000-0002-7574-1298
L. Di Venere https://orcid.org/0000-0003-0703-824X
A. Domínguez https://orcid.org/0000-0002-3433-4610
V. Fallah Ramazani https://orcid.org/0000-0001-8991-7744
E. C. Ferrara https://orcid.org/0000-0001-7828-7708
A. Fiori https://orcid.org/0000-0003-3174-0688
Y. Fukazawa https://orcid.org/0000-0002-0921-8837
S. Funk https://orcid.org/0000-0002-2012-0080
P. Fusco https://orcid.org/0000-0002-9383-2425
V. Gammaldi https://orcid.org/0000-0003-1826-6117
F. Gargano https://orcid.org/0000-0002-5055-6395
S. Garrappa https://orcid.org/0000-0003-2403-4582
D. Gasparrini https://orcid.org/0000-0002-5064-9495
N. Giglietto https://orcid.org/0000-0002-9021-2888
M. Giroletti https://orcid.org/0000-0002-8657-8852
D. Green https://orcid.org/0000-0003-0768-2203
S. Guiriec https://orcid.org/0000-0001-5780-8770
D. Horan https://orcid.org/0000-0001-5574-2579
X. Hou https://orcid.org/0000-0003-0933-6101
T. Kayanoki https://orcid.org/0000-0002-6960-9274
M. Kuss https://orcid.org/0000-0003-1212-9998
S. Larsson https://orcid.org/0000-0003-0716-107X
L. Latronico https://orcid.org/0000-0002-0984-1856
T. Lewis https://orcid.org/0000-0002-9854-1432
J. Li https://orcid.org/0000-0003-1720-9727
F. Longo https://orcid.org/0000-0003-2501-2270
F. Loparco https://orcid.org/0000-0002-1173-5673
B. Lott https://orcid.org/0000-0003-2186-9242
P. Lubrano https://orcid.org/0000-0003-0221-4806
S. Maldera https://orcid.org/0000-0002-0698-4421
A. Manfreda https://orcid.org/0000-0002-0998-4953
G. Martí-Devesa https://orcid.org/0000-0003-0766-6473
M. N. Mazziotta https://orcid.org/0000-0001-9325-4672
I. Mereu https://orcid.org/0000-0003-0219-4534
N. Mirabal https://orcid.org/0000-0002-7021-5838
W. Mitthumsiri https://orcid.org/0000-0002-3776-072X
T. Mizuno https://orcid.org/0000-0001-7263-0296
M. E. Monzani https://orcid.org/0000-0002-8254-5308
A. Morselli https://orcid.org/0000-0002-7704-9553
I. V. Moskalenko https://orcid.org/0000-0001-6141-458X
M. Negro https://orcid.org/0000-0002-6548-5622
J. F. Ormes https://orcid.org/0000-0002-7220-6409
H. Peña-Herazo https://orcid.org/0000-0003-0032-9538
M. Persic https://orcid.org/0000-0003-1853-4900
M. Pesce-Rollins https://orcid.org/0000-0003-1790-8018
V. Petrosian https://orcid.org/0000-0002-2670-8942
H. Poon https://orcid.org/0000-0002-6004-4270
T. A. Porter https://orcid.org/0000-0002-2621-4440
S. Rainò https://orcid.org/0000-0002-9181-0345
B. Rani https://orcid.org/0000-0001-5711-084X
M. Razzano https://orcid.org/0000-0003-4825-1629
S. Razzaque https://orcid.org/0000-0002-0130-2460
A. Reimer https://orcid.org/0000-0001-8604-7077
O. Reimer https://orcid.org/0000-0001-6953-1385
L. Scotton https://orcid.org/0000-0002-0602-0235
C. Sgrò https://orcid.org/0000-0001-5676-6214
D. J. Suson https://orcid.org/0000-0003-2911-2025
D. F. Torres https://orcid.org/0000-0002-1522-9065
J. Valverde https://orcid.org/0000-0002-8090-6528

References

Abdo, A. A., Ackermann, M., Agudo, I., et al. 2010a, ApJ, 716, 30
Abdo, A. A., Ackermann, M., Ajello, M., et al. 2010b, ApJS, 188, 405
Abdollahi, S., Acero, F., Ackermann, M., et al. 2020, ApJS, 247, 33
Abdollahi, S., Acero, F., Baldini, L., et al. 2022, ApJS, 260, 53
Ackermann, M., Ajello, M., Allafort, A., et al. 2011, ApJ, 743, 171
Ackermann, M., Ajello, M., Atwood, W. B., et al. 2015, ApJ, 810, 14
Ajello, M., Angioni, R., Axelsson, M., et al. 2020, ApJ, 892, 105
Atwood, W. B., Abdo, A. A., Ackermann, M., et al. 2009, ApJ, 697, 1071
Ballet, J., Burnett, T. H., Digel, S. W., & Lott, B. 2020, arXiv:2005.11208
Britzen, S., Vermeulen, R. C., Campbell, R. M., et al. 2008, A&A, 484, 119
de Menezes, R., Nemmen, R., Finke, J. D., Almeida, I., & Rani, B. 2020, MNRAS, 492, 4120
Desai, A., Marchesi, S., Rajagopal, M., & Ajello, M. 2019, ApJS, 241, 5
Finke, J. D. 2013, ApJ, 763, 134
Fukazawa, Y., Matake, H., Kayanoki, T., Inoue, Y., & Finke, J. 2022, ApJ, 931, 138
Goldoni, P., Pita, S., Boisson, C., et al. 2021, A&A, 650, A106
Grandi, P., Capetti, A., & Baldi, R. D. 2016, MNRAS, 457, 2
Järvelä, E., Berton, M., Ciroi, S., et al. 2020, A&A, 636, L12
Lott, B., Gasparrini, D., & Ciprini, S. 2020, arXiv:2010.08406
Martí, J., Sánchez-Ayaso, E., Luque-Escamilla, P. L., et al. 2020, MNRAS, 492, 4291
Meyer, E. T., Fossati, G., Georganopoulos, M., & Lister, M. L. 2011, ApJ, 740, 98
Nalewajko, K., & Gupta, M. 2017, A&A, 606, A44
NASA/IPAC Extragalactic Database (NED) 2019, NASA/IPAC Extragalactic Database (NED) (Pasadena, CA: Caltech), https://ned.ipac.caltech.edu/
Paliya, V. S. 2021, ApJL, 918, L39
Paliya, V. S., Domínguez, A., Ajello, M., Olmo-García, A., & Hartmann, D. 2021, ApJS, 253, 46
Paliya, V. S., Domínguez, A., Cabello, C., et al. 2020a, ApJL, 903, L8
Paliya, V. S., Pérez, E., García-Benito, R., et al. 2020b, ApJ, 892, 133
Peña-Herazo, H. A., Marchesini, E. J., Alvarez Crespo, N., et al. 2017, Ap&SS, 362, 228
Peña-Herazo, H. A., Massaro, F., Chavushyan, V., et al. 2019, Ap&SS, 364, 85
Peña-Herazo, H. A., Amaya-Almazán, R. A., Massaro, F., et al. 2020, A&A, 643, A103
Peña-Herazo, H. A., Massaro, F., Gu, M., et al. 2021a, AJ, 161, 196
Peña-Herazo, H. A., Massaro, F., Gu, M., et al. 2021b, AJ, 162, 76
Peña-Herazo, H. A., Paggi, A., Garcia-Perez, A., et al. 2021c, AJ, 162, 177
Rajagopal, M., Marchesi, S., Kaur, A., et al. 2021, ApJS, 254, 26
Saldana-Lopez, A., Domínguez, A., Pérez-González, P. G., et al. 2021, MNRAS, 507, 5144
van Velzen, S., Falcke, H., Schellart, P., Nierstenhöfer, N., & Kampert, K.-H. 2012, A&A, 544, A18
Wrobel, J. M., & Heeschen, D. S. 1984, ApJ, 287, 41